Calculation of mass transfer coefficients for corrosion prediction in two-phase gas-liquid pipe flow

Luciano D. PAOLINELLI[1] and Srdjan NESIC[1]

[1] Institute for Corrosion and Multiphase Technology
Department of Chemical and Biomolecular Engineering, Ohio University,
342 W. State Street, Athens OH, USA,
paolinel@ohio.edu
nesic@ohio.edu

Abstract

Internal corrosion in industrial environments involving gas-liquid flow can be a serious concern. For example, in the oil and gas industry, corrosive water phase is usually transported in tubes and pipes along with hydrocarbon and gas phases. These gas-liquid flows develop complex flow patterns where the liquid phase can distribute in quite different ways (as stratified layers, intermittent slugs, annular film, etc.) depending on the gas and liquid flow rates and pipe inclination. In these circumstances, the water phase can flow at very high velocities compare to either single-phase water flow or two-phase hydrocarbon-water flow. High water velocities usually lead to high mass transfer rates that can accelerate corrosion of the metallic pipe surface. In general, proper calculation of corrosion rates via mechanistic electrochemical models requires the knowledge of the mass transfer rate of corrosive species. However, there are very few studies in the open literature that show specific experimental data or propose ways to compute mass transfer rates in gas-liquid flow; particularly, for large pipe diameters. This study introduces a methodology for the estimation of mass transfer rates in gas-liquid flow based on the Chilton-Colburn analogy, eddy diffusivity, and mechanistic gas-liquid flow modeling. The proposed mechanistic models covers a wide range of fluid's properties and flow rates, different flow regimes and pipe inclinations, and show good agreement with mass transfer experimental data from large-scale gas-liquid flow.

Keywords: Gas-liquid flow; mass transfer; flow patterns; mechanistic modeling

Introduction

Internal corrosion can be an important problem in industry that deals with production and/or transportation of liquid and gas phases. In the oil and gas industry, hydrocarbons are usually produced with gas and corrosive water (carrying dissolved CO_2 and H_2S), and transported in tubes and pipes. Gas lines also deal with hydrocarbon and water condensation, the latter may lead to corrosion problems as well as "black powder" formation that are all undesired [1].

Gas-liquid flows can develop a wide variety of flow patterns in which the liquid phase can distribute in different ways. For example, in horizontal flow, relatively low superficial liquid velocities, and low to moderate superficial gas velocities lead to stratified flow of gas at the top and liquid at the bottom of the pipe with a smooth or wavy gas liquid interface ("ST" regime in Figure 1). The operating region for stratified flow drastically narrows even for very small upward inclination angles (e.g., ~1 degree) favoring the occurrence of intermittent flow regime or slug flow [2].

Slug flow regime occurs at moderate superficial liquid velocities and a wide range of superficial gas velocities as shown as "SL" regime in Figure 1. This flow regime can develop very high liquid velocities since the translational velocity of liquid slugs is proportional to the

summation of the superficial velocities of the liquid and gas phases. In horizontal flow, the velocity of the film liquid in the gas pocket zones is relatively low compared to the liquid slug. However, liquid film velocities can be relatively high in inclined and vertical upward flows where the liquid film moves counter current while the gas pockets flow with the main stream.

When superficial gas velocities are high and the liquid holdup is not high enough to bridge the entire pipe cross-section to produce slugs, the gas phase flows through the core of the pipe and entrains liquid droplets which are simultaneously deposited all around the pipe circumference, producing an annular film. This flow regime is called annular mist ("AM" regime in Figure 1). Momentum transfer from the mixed gas-liquid core flow to the liquid film can be significant. For high superficial liquid velocities, the gas phase is fully entrained and dispersed as bubbles in the liquid phase, which is the flow regime indicated as "DB" in Figure 1.

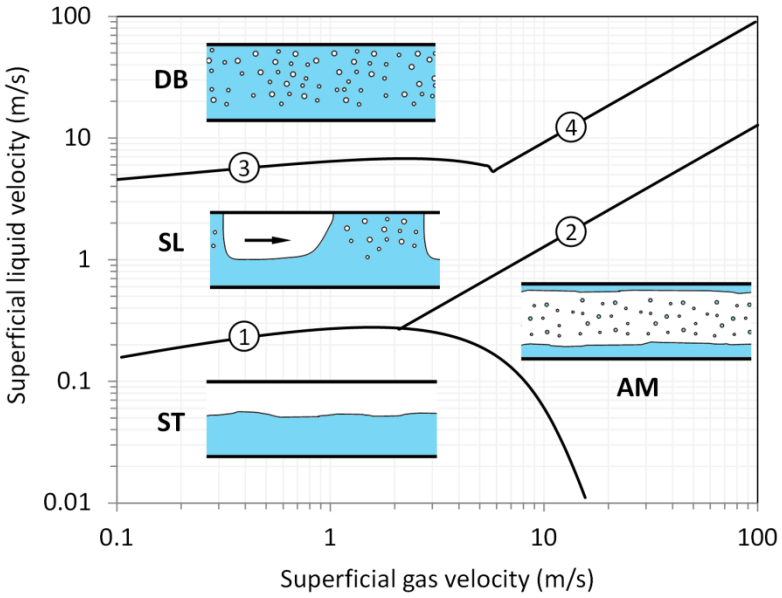

Figure 1. Calculated gas-liquid flow map. AM: Annular mist flow, DB: Dispersed bubble flow, SL: Slug/intermittent flow, ST: Stratified flow. Horizontal flow, d=0.1 m, ρ_l=1000 kg/m^3, μ_l=1 mPa.s, ρ_g=10 kg/m^3, μ_l=0.018 mPa.s.

Some of the gas-liquid flow regimes mentioned above (e.g., SL and AM) can develop very high liquid velocities compare to either single-phase water flow or other two-phase hydrocarbon-water flows. These high liquid velocities lead to high wall shear stresses and high mass transfer rates that can significantly accelerate corrosion of metallic pipe surfaces. In general, mechanistic models to calculate corrosion rate are based on the electrochemical reactions occurring at the pipe surface; e.g., oxidation of iron and reduction of hydronium ions. For the latter or any other aggressive species under consideration, it is crucial to define mass transfer rates with reasonable accuracy in order to obtain good prediction of corrosion rates [3, 4].

The characteristics of mass transport from a bulk liquid phase to a solid pipe wall in multiphase gas-liquid flow have been studied previously, mainly by means of electrochemical techniques such as the measurements of limiting currents on arrangements of inert electrodes

flush mounted at the pipe surface [5-10]. Only a few studies were performed in pipes with large diameter (e.g., 0.1m) which are more representative of the flows encountered in the oil and gas industry [5, 8, 9]. Regarding the calculation of mass transfer rates in large scale gas-liquid pipe flow, there have been attempts to build correlations derived from the one proposed by Berger and Hau [11] for single phase pipe flow [8, 12]. Although these suggested correlations use dimensionless numbers derived from the Chilton-Colburn relationship, they are not mechanistic and oversimplify the effect of the wall shear stress exerted by the liquid phase on mass transfer rate and do not cover all flow regimes.

The objective of this study is to introduce a methodology for the estimation of mass transfer rates in multiphase gas-liquid flow. Two different approaches are used, based on the Chilton-Colburn analogy and eddy diffusivity, as well as on mechanistic gas-liquid flow modeling to obtain liquid flow characteristics (liquid velocity and wall shear stress) in the different flow regimes. Mass transfer calculation results are discussed and compared with available experimental data obtained in large-scale gas-liquid flow with different flow patterns.

Mass transfer model

Fundamental mass transfer relationship

Mass transfer rates in fully developed turbulent boundary layer can be related to the wall shear stresses by the Chilton-Colburn analogy [13]:

$$\left(\frac{f}{2}\right)^n = \frac{Sh}{Re\, Sc^{1/3}}; \tag{1}$$

$$Sc = \frac{\mu}{\rho D}; \tag{2}$$

$$Sh = \frac{kd}{D}; \tag{3}$$

$$Re = \frac{\rho u d}{\mu} \tag{4}$$

where Sc, Sh and Re are the Schmidt, Sherwood and Reynolds numbers, respectively, D is the diffusion coefficient of a given specie in the studied fluid, d is a characteristic length that for single phase pipe flow is the internal pipe diameter, f is the Fanning friction factor, k is the mass transfer coefficient, u is the mean velocity of the fluid, μ is the fluid dynamic viscosity, and ρ is the fluid density. The exponent n is equal to 1 according to [13]. However, some authors suggested that the exponent can be between 1 and 0.5 [11, 14, 15].

Mass transfer coefficient can be calculated directly from (1) as:

$$k = \left(\frac{f}{2}\right)^n u\, Sc^{-2/3} = \left(\frac{\tau}{\rho u^2}\right)^n u\, Sc^{-2/3} \tag{5}$$

where τ is the wall shear stress exerted by the fluid.

The main advantage of equation (5) is that, regardless of the geometrical characteristics of the flow under study (e.g., pipe flow, rotating cylinder, jet impingement, etc.), it allows the estimation of the mass transfer rate at any given boundary layer as long as the wall shear

stress and the mean flow velocity are known. For example, Figure 2 shows the Sherwood numbers for hydraulically smooth pipe and rotating cylinder flows calculated by equation (5) (black dashed lines) using the friction factors described in the Appendix (equations (A.1) and (A.3), respectively), and compares them with the Sherwood numbers calculated using the widely accepted Berger and Hau [11] and Eisenberg et al. [16] correlations (equations (A.2) and (A.6), respectively, see Appendix). An exponent of 0.96 is found to be the most appropriate to estimate the mass transfer characteristics of both flows in the range $200 \leq Sc \leq 10{,}000$ with an average absolute error $\leq 10\%$.

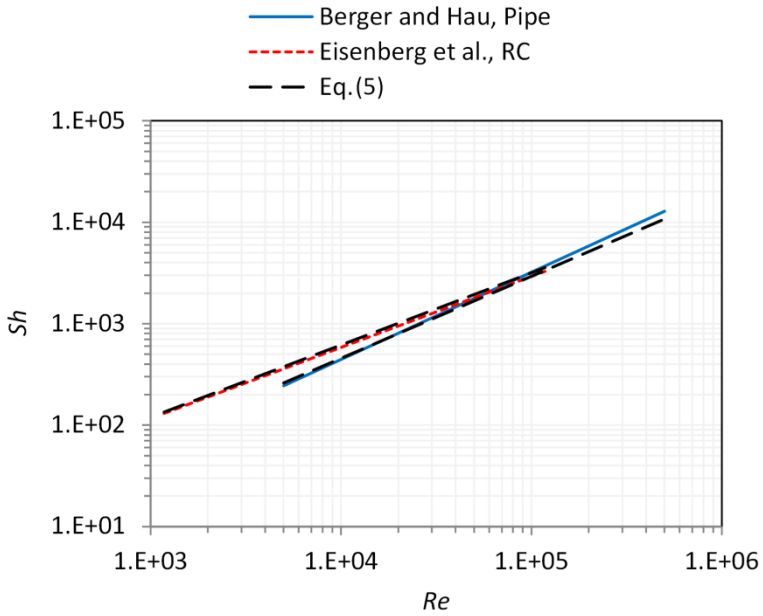

Figure 2. Sherwood numbers for pipe and rotating cylinder (RC) calculated using equation (5) compared to well-stablished correlations. Sc=1000, d=0.1 m, $2r$=0.015m, ρ_l=1000 kg/m^3, μ_l=1 mPa.s.

Mass transfer in gas-liquid pipe flow

Mass transfer calculation via the Chilton-Colburn fundamental relationship:

From equation (5), it is obvious that the ionic mass transfer characteristics of the liquid phase are directly related to the velocity of the liquid (u_l) and wall shear stress (τ_l) exerted by the liquid on the pipe wall:

$$k = \left(\frac{\tau_l}{\rho_l {u_l}^2}\right)^n u_l \, Sc^{-2/3} \qquad (6)$$

where ρ_l is the density of the liquid and Sc is based on the liquid physical properties. In order to estimate the values of u_l and τ_l for a determined set of liquid and gas flow rates and pipe geometry (e.g., diameter and inclination) the use of a multiphase gas-liquid model is needed in which the liquid flow characteristics are dependent of the gas-liquid flow pattern.
Equation (6) can be directly used to obtain mass transfer coefficients in the case of stratified, annular and dispersed bubble flow, by simply inputting the liquid velocity and wall shear stress obtained from, for example, the gas-liquid model presented in the Appendix.

In the case of slug flow, the mass transfer coefficient is computed as the average of the mass transfer coefficients of the liquid slug and film regions:

$$k = k_{\mathrm{s}} + k_{\mathrm{f}} = \left[\left(\frac{\tau_{\mathrm{ls}}}{\rho_{\mathrm{l}} {u_{\mathrm{t}}}^2}\right)^n u_{\mathrm{t}} \beta_{\mathrm{s}} + \left(\frac{|\tau_{\mathrm{lf}}|}{\rho_{\mathrm{l}} {u_{\mathrm{lf}}}^2}\right)^n |u_{\mathrm{lf}}|(1-\beta_{\mathrm{s}})\right] Sc^{-2/3} \quad (7)$$

where u_{t} is the velocity of the liquid slug front, u_{lf} is the velocity of the liquid film, τ_{ls} and τ_{lf} are the wall shear stresses of the liquid slug and the liquid film, respectively; and β_{s} is the relative length of the liquid slug as shown in Figure A.1 in the Appendix. Note that the velocity and the wall shear stress of the liquid film are computed as absolute value since they can be negative (counter current flow) in inclined and vertical flows.

Mass transfer computation in systems with simultaneous reactions at the pipe wall and in the liquid:

In cases where species react with the solid surface as well as with other species in the fluid, e.g., as the case of hydronium ions in CO_2 or H_2S corrosion [3, 17, 18], the computation of the concentration of a given specie at the pipe wall will depend not only on its molecular diffusion and the transport characteristics of the fluid flow boundary layer but also on the consumption or generation of this specie close to the solid wall. Therefore, specific functions to determine turbulent transport characteristics in function of the distance from the solid wall are needed. The mass transfer rate in the normal direction (y) of a solid wall in steady state turbulent flow can be written as:

$$N = D\frac{\partial C}{\partial y} + \overline{v'C'} \quad (8)$$

where N is the mass flux, $C'$is the concentration fluctuation, and v' is the flow velocity fluctuation. The term $\overline{v'C'}$ can be modeled as and eddy diffusivity that is added to the molecular diffusion:

$$N = (D + D_{\mathrm{t}})\frac{\partial C}{\partial y} \quad (9)$$

where the turbulent diffusion of mass is defined by analogy to the eddy diffusion of momentum as [19]:

$$D_{\mathrm{t}} = \left(\frac{y^+}{C_{\mathrm{t}}}\right)^3 \frac{\mu_{\mathrm{l}}}{\rho_{\mathrm{l}}} \quad (10)$$

where C_{t} is a constant that can range from 8.8 to 14.5 according to different authors [19, 20], and y^+ is the dimensionless distance from the solid wall:

$$y^+ = y\frac{\rho_{\mathrm{l}} u^*}{\mu_{\mathrm{l}}} \quad (11)$$

where u^* is the friction velocity calculated as $\sqrt{\tau_{\mathrm{l}}/\rho_{\mathrm{l}}}$.

Equation (11) is valid provided that the diffusion boundary layer (δ) is smaller than the viscous sublayer of the liquid flow ($\delta^+ < 5$) which, in general, is true for Sc >100.

The mass flux at the solid wall (N_w) can be calculated solving the equation (9) within a domain larger than δ. The mass transfer coefficient is then defined as:

$$k = \frac{N_w}{(C_w - C_b)} \tag{12}$$

where C_b and C_w are the concentrations of a given specie at the bulk of the fluid and at the wall surface, respectively.

The use of equations (9) and (10) is direct in the case of gas-liquid flows with stratified, annular and dispersed bubble flow patterns via the use of the actual wall shear stress of the liquid phase for the calculation of the friction velocity in equation (11). However, for slug flow, the hydrodynamic boundary layers of the liquid film and liquid slug can be very different. Moreover, in some operating conditions period between slugs can be smaller than a second, which might be a relatively short time to fully develop the hydrodynamic and diffusion boundary layers. Regardless of these facts, the hydrodynamic boundary layer in slug flow can be characterized by an average friction velocity:

$$\overline{u^*} = u^*_{ls}\,\beta_s + u^*_{lf}\,(1 - \beta_s) = \sqrt{\frac{\tau_{ls}}{\rho_l}}\,\beta_s + \sqrt{\frac{|\tau_{lf}|}{\rho_l}}\,(1 - \beta_s) \tag{13}$$

Then, $\overline{u^*}$ is directly used in equation (11) to compute y^+.

Results and discussion

Ionic mass transfer in gas-water pipe flow

The models proposed above are compared with experimental data of ionic mass transfer from Langsholt et al. [5] and Wang et al. [8] obtained in large-scale gas-water flows with stratified and slug flow patterns.

Langsholt et al. used an inclinable multiphase flow loop with an internal diameter 0.1 m and a length (l) of 15 m. The gas phase was sulphur hexafluoride (SF_6) with reported density of 18.6 kg/m^3 and calculated viscosity of 1.5×10^{-2} mPa.s at operating conditions (20°C and ~3bar). The liquid phase was an aqueous solution 1 wt.% Na_2SO_4 with density of 1006 kg/m^3 and viscosity of 1 mPa.s. Ionic mass transfer rates were measured by the limiting current method using an electrochemical probe flush mounted at the bottom of the test section and oxygen reduction as the monitored reaction with a Schmidt number of 473. Liquid holdup was also measured using gamma densitometry. The covered operating conditions and visualized flow patterns, as well as the measured average mass transfer rates and liquid holdups are listed in Table A.1 in the Appendix.

Wang, et al. also used a multiphase flow loop with an internal diameter 0.1m and a length (l) of 15 m. The gas phase was nitrogen with estimated density of 1.15 kg/m^3 and viscosity of 1.7×10^{-2} mPa.s at operating conditions (20°C and ~1.5bar). The liquid phase was an aqueous solution 0.01M potassium ferri/ferrocyanide and 1M NaOH for the mass transfer measurements by the limiting current method. The calculated density and viscosities of the solution are 1043 kg/m^3 and 1.1 mPa.s, respectively; and the estimated Schmidt number is

1620 [21]. The used operating conditions, observed flow patterns, and measured average mass transfer rates are listed in Table A.2 in the Appendix.

Figure 3 shows the comparison of the measured mass transfer coefficients in different conditions and flow patterns with the ones calculated with equations (6) and (7) fed by the gas-liquid flow model presented in the Appendix. The agreement between the proposed model and the experimental data is fairly good with an absolute error of 23% and most of the data lying within the ±30% error bounds. The conditions that showed more error were the ones from 2° upward slug flows from Langsholt et al. A possible reason for these discrepancies might be related to an over prediction of counter current liquid velocities in the liquid film by the simplified gas-liquid model in the Appendix.

Mass transfer predictions using the introduced mechanistic model are an improvement over semi-empirical correlations for gas-liquid flow offered in the literature, which are mostly developed based on data from air-water flows in relatively small diameter pipes (e.g., 0.025m), as reviewed in the recent works of Dong and Hibiki [22, 23]. Most of these correlations are limited for horizontal or upwards/downwards vertical flows, as well as relatively low superficial gas and liquid Reynolds numbers, making them unfeasible for large scale flows (e.g., large diameters and gas and liquid flow rates) with different inclinations and upward or downward orientations. The correlation that performs better over the current experimental data with an average absolute error of 20% is the one from Dong and Hibiki [22], which is based on vertical flows. However, it underestimates by about 70% experimental mass transfer rates measured in flows with liquid holdups smaller than 10%.

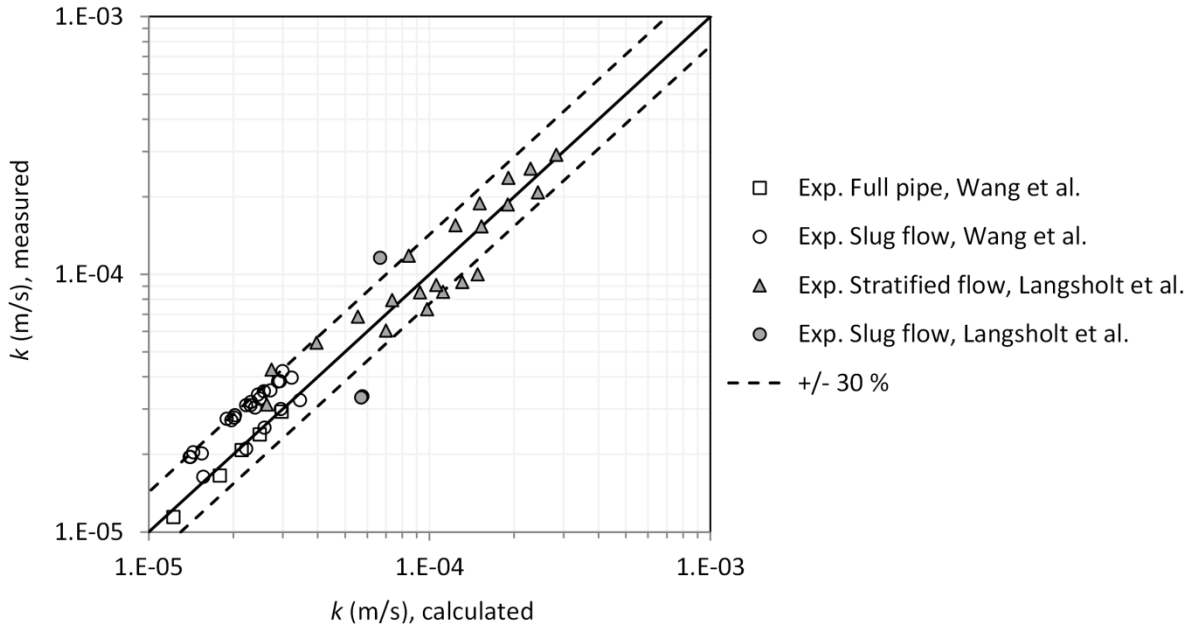

Figure 3. Comparison between experimental mass transfer coefficients for large-scale gas-liquid pipe flow with different flow patterns and mass transfer coefficients calculated with equations (6) and (7).

As discussed above, in cases where the modeling of transport of species also depend on chemical reactions occurring in the fluid near the pipe wall, it is more appropriate to use the

approach described in equation (9). This equation was solved numerically for all the experimental cases applying the finite difference method using at least 20 elements in the diffusion layer (δ) and a total domain with a length larger than 4δ. Mass transfer coefficients were then calculated with equation (12). Equation (10) for turbulent diffusion was assessed using coefficients suggested by Davies (C_t=8.85, [20]) and Lin et al. (C_t=14.5, [19]); the eddy diffusivity functions suggested by Notter and Sleicher [24] and Aravinth [25] were also evaluated. Figure 4 shows the mass transfer rates calculated in single phase flow using the eddy diffusivity approach compared to the Berger and Hau correlation. Although the eddy diffusivity approach follows reasonably well the slope with Reynolds number seen in Berger and Hau's correlation, the expressions suggested by Davies, Notter and Sleicher, and Aravinth overestimate mass transfer rates by an average of more than 50%. The Lin et al. formulation gives better results with an average overestimation of 21%.

Experimental mass transfer coefficients in gas-liquid flow were then modeled using the Lin et al. formulation as shown in Figure 5. Calculations show an important overestimation of mass transfer rates with an average absolute error of 34%. Moreover, about 40% of the data lie out of the 30% error bound including the single phase flow data of Wang. et al. (42% average error). This behavior was somehow expected since Lin et al.'s expression overestimates mass transfer rates in single phase flow by at least an average of 20% as previously shown in Figure 4. An increase in the coefficient C_t in equation (10) to a value of 18.4 leads to an average absolute error of about 6% respect to Berger and Hau's correlation, and an average absolute error of 19% respect to the experimental data from gas-liquid flow as shown in Figure 6. Higher values of C_t no longer improve the average absolute error on the experimental data from multiphase flow, and lead to underestimation of mass transfer in single phase by more than 10% in average.

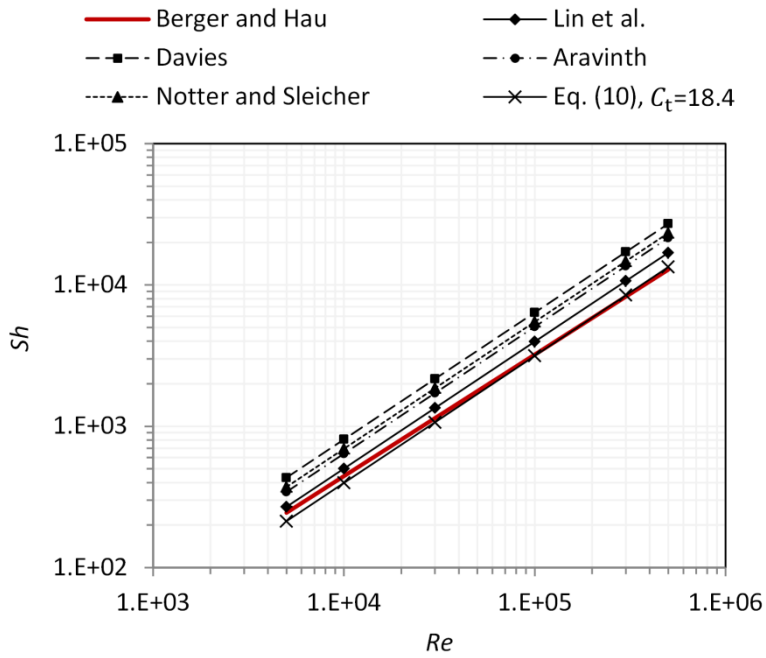

Figure 4. Comparison between mass transfer rates for single phase pipe wall calculated with the eddy diffusivity approach and Berger and Hau's correlation. Sc=1000, d=0.1 m, ρ_l=1000 kg/m^3, μ_l=1 mPa.s.

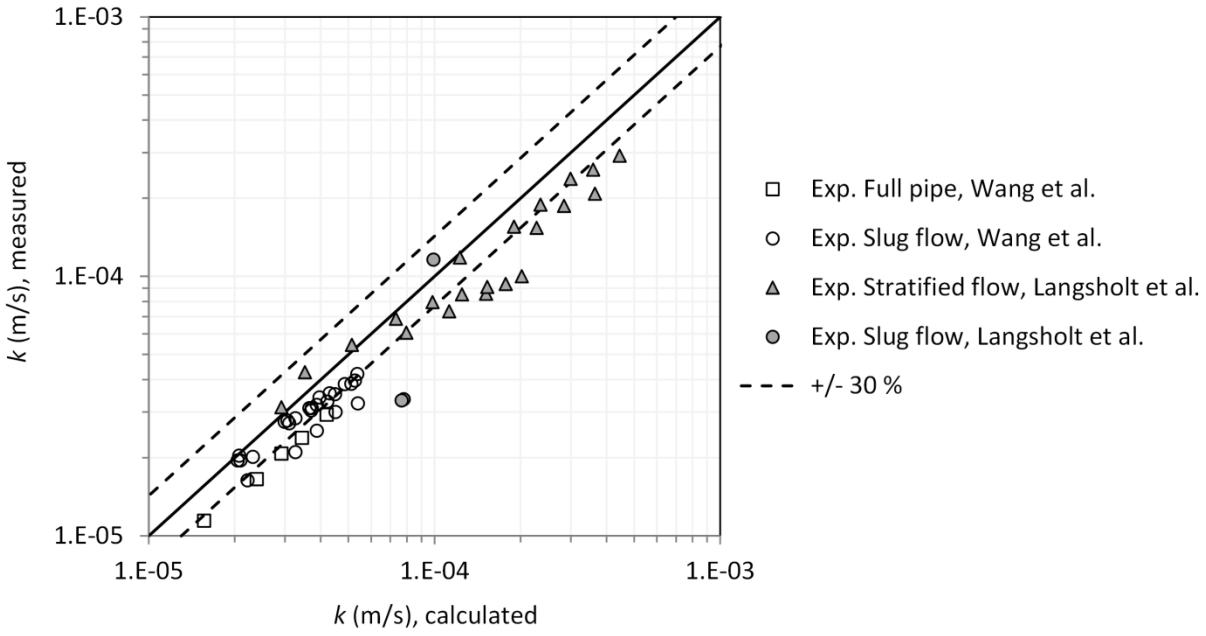

Figure 5. Comparison between experimental mass transfer coefficients for large-scale gas-liquid pipe flow with different flow patterns and mass transfer coefficients calculated with the eddy diffusivity approach using Lin et al.'s formulation.

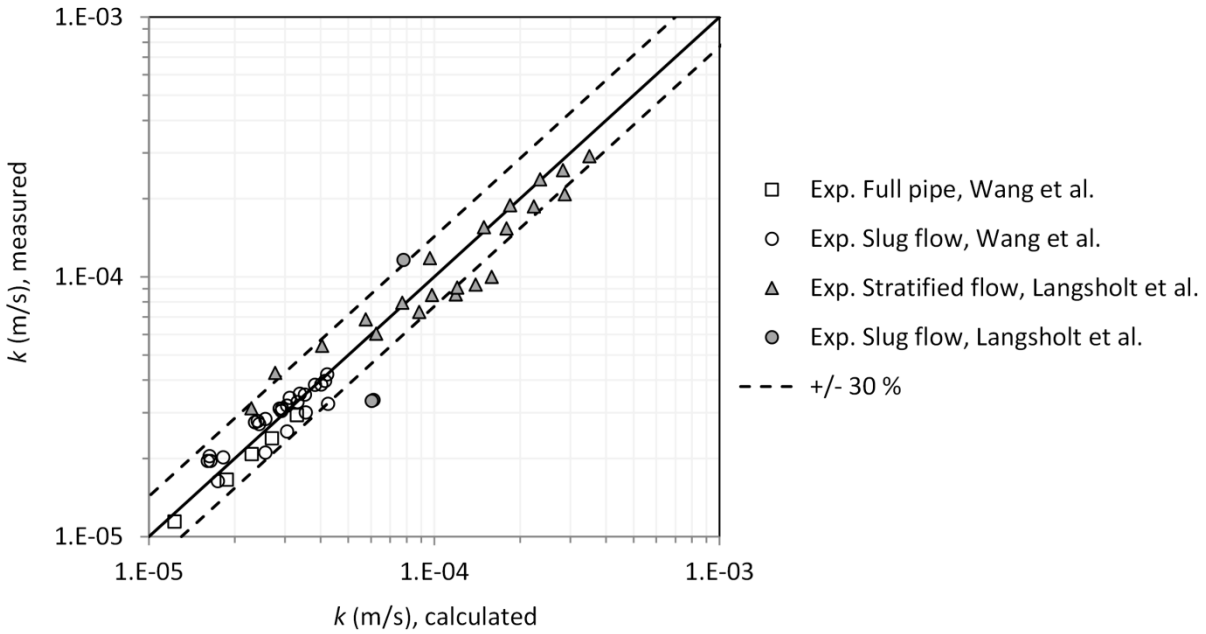

Figure 6. Comparison between experimental mass transfer coefficients for large-scale gas-liquid pipe flow with different flow patterns and mass transfer coefficients calculated with the eddy diffusivity approach using equation (10) with C_t=18.4.

Ionic mass transfer in gas-oil-water and oil-water pipe flow

Generally, flows in the oil and gas industry contain significant fractions of liquid hydrocarbons. In the case of gas-oil-water flows, the produced oil and water phases that can flow either separated or mixed. If flow conditions (e.g., gas, oil and water flow rates) are

viable to produce the full entrainment of the water in the oil phase, the pipe wall will not likely be water wet and ionic mass transfer would be suppressed [26, 27]. However, if water either segregates from or is the continuous phase of the liquid mix, mass transfer rates can be similar to the ones corresponding to gas-water flow without hydrocarbon [9]. Therefore, calculation of mass transfer rates in gas-oil-water flow can still be done using equations (6) and (7) (fundamental Chilton-Colburn relationship) or the eddy diffusivity approach, using liquid velocities and wall shear stresses calculated with the following liquid mixture properties:

$$\rho_{\mathrm{lm}} = \rho_{\mathrm{o}}(1-\varepsilon_{\mathrm{w}}) + \rho_{\mathrm{w}}\varepsilon_{\mathrm{w}} \tag{14}$$

$$\mu_{\mathrm{lm}} \cong \begin{cases} \mu_{\mathrm{o}} & \varepsilon_{\mathrm{w}} < IP \\ \mu_{\mathrm{w}} & \varepsilon_{\mathrm{w}} > IP \end{cases} \tag{15}$$

where ρ_{lm} and μ_{lm} are the density and the viscosity of the liquid mixture, respectively; ρ_{o} and μ_{o} are the density and viscosity of the oil phase, ρ_{w} and μ_{w} are the density and viscosity of the water phase, IP is the phase inversion of the oil-water mixture based on the water volume content (for crude oil can be approximated as 0.5); and ε_{w} is the volumetric water fraction in the liquid mix, which can be approximated as the water cut (no slip between oil and water phases) :

$$\varepsilon_{\mathrm{w}} = \frac{u_{\mathrm{sw}}}{u_{\mathrm{sw}}+u_{\mathrm{so}}} = \frac{u_{\mathrm{sw}}}{u_{\mathrm{sl}}} \tag{16}$$

where u_{so} and u_{sw} are the superficial velocities of oil and water; respectively, which sum gives the total superficial liquid velocity u_{sl}. Schmidt number is obviously calculated using the physical properties of the water phase.

In the case of oil-water flow (negligible or no gas phase present), the calculation of mass transfer rates is performed similarly as to gas-liquid flow. However, an oil-water flow model is required for the estimation of the velocity and wall shear stress of the water phase.

Summary and conclusions

Two different approaches for mass transfer estimation in multiphase gas-liquid flow have been introduced and compared against experimental data from large-scale flows with different flow regimes. In general, the agreement of the offered mass transfer models with the available experimental data is reasonably good for all the different assessed flow patterns; especially, in slug flow where the hydrodynamic and diffusion boundary layers fluctuate in relatively short periods.

Direct computation of mass transfer coefficients can be done with fair accuracy for a wide variety of flows (single phase pipe and rotating cylinder, and two-phase gas-liquid pipe) by using the fundamental Chilton-Colburn with an exponent of 0.96 on the friction factor.

Mass transfer calculation via the eddy diffusivity approach tend to overestimate mass transfer rates for single and multiphase flow when some of the classic formulations in the literature. The use of the classic cubic variation of eddy diffusivity with a coefficient of 18.4 affecting the dimensionless wall distance; instead of the smaller values suggested in the literature,

proved to be the most appropriate to predict mass transfer rates in single and multiphase flow with fair accuracy.

The main strength of the proposed models is their mechanistic nature, which allows their use in systems with wide range of physical properties (different gas and liquid densities and viscosities) and pipe characteristics (different diameters, inclination, smooth and rough surfaces). Moreover, better results can surely be achieved if liquid flow characteristics are estimated using multiphase flow models more advanced and refined than the one currently offered. This is a significant improvement over semi-empirical correlations suggested in the literature that are usually tuned for limited ranges of fluid's properties and flow rates, making them unreliable for general use. In addition, these correlations cannot be applied to cases where species react in the fluid as well as at the pipe wall.

Acknowledgements

The authors want to thank the financial support from the multiple companies that participate of JIPs and other research projects at the Institute for Corrosion and Multiphase Technology at Ohio University.

Appendix

Experimental data used in the model validation

Table A.1. Experimental conditions, measured liquid holdup and average mass transfer rates in horizontal and slightly inclined flow from Langsholt et al. [5].

Flow pattern	u_{sl} [m/s]	u_{sg} [m/s]	β [°]	α_l [%]	Sh
Strat.-wavy	0.021	2.14	0	6.1	1489
Strat.-wavy	0.019	4.11	0	2	2884
Strat.-wavy	0.025	6.34	0	1.2	3491
Strat.-wavy	0.25	6.06	0	11.1	4076
Strat.-wavy	0.25	7.1	0	9.5	4450
Strat.-wavy	0.25	8.18	0	8.2	4762
Strat.-wavy	0.25	5.05	0	12.9	4053
Strat.-wavy	0.25	4.1	0	15.4	3788
Strat.-wavy	0.25	3	0	19.4	3265
Strat.-wavy	0.25	2.03	0	27.2	2587
Strat.-wavy	0.25	0.96	0	42	2034
Strat.-wavy	2	3	2	50	7404
Strat.-wavy	2	5	2	31	8986
Strat.-wavy	2	7	2	21	11300
Strat.-wavy	2	9	2	17	12275
Strat.-wavy	2	12	2	13	13888
Strat.-wavy	1	3	2	42	5627
Strat.-wavy	1	7	2	19	7326
Strat.-wavy	1	9	2	14	8892
Strat.-wavy	1	12	2	9	9913
Strat.-wavy	0.78	5	2	43	4333

Slug	0.78	2	2	30	5518
Slug	0.13	2	2	26	1598
Slug	0.1	2	2	25	1582

Table A.2. Experimental conditions and measured average mass transfer rates in horizontal flow from Wang et al. [8].

Flow pattern	u_{sl} [m/s]	u_{sg} [m/s]	Sh
Full liquid	0.5	0	1756
Full liquid	0.8	0	2543
Full liquid	1	0	3189
Full liquid	1.2	0	3669
Full liquid	1.5	0	4509
Slug	0.5	0.6	2514
Slug	0.8	0.6	3232
Slug	1	0.6	3903
Slug	1.2	0.6	4613
Slug	1.5	0.6	4986
Slug	0.5	1.4	3001
Slug	0.8	1.4	4272
Slug	1	1.4	4672
Slug	1.2	1.4	5451
Slug	1.5	1.4	6101
Slug	0.5	2.4	3001
Slug	0.8	2.4	4168
Slug	1	2.4	4777
Slug	1.2	2.4	5255
Slug	1.5	2.4	5904
Slug	0.5	3.6	3131
Slug	0.8	3.6	4227
Slug	1	3.6	4777
Slug	1.2	3.6	5060
Slug	1.5	3.6	5919
Slug	0.5	4.8	3102
Slug	0.8	4.8	4361
Slug	1	4.8	4911
Slug	1.2	4.8	5406
Slug	1.5	4.8	6466

Turbulent single-phase pipe flow

Friction factor, Blasius equation:

$$f = 0.046Re^{-0.2} \qquad Re > 2100 \tag{A.1}$$

Mass transfer correlation, Berger and Hau [11]:

$$Sh = 0.0165Re^{0.86}Sc^{0.33}; \quad 8 \times 10^3 \leq Re \leq 2 \times 10^5; \quad 10^3 \leq Sc \leq 6 \times 10^3 \tag{A.2}$$

Turbulent single-phase rotating cylinder flow

Friction factor [16]:

$$\frac{f}{2} = 0.079 {Re_c}^{-0.3}; \qquad 1000 \leq Re_{rc} \leq 100{,}000 \tag{A.3}$$

$$Re_{rc} = \frac{2\rho r U_{rc}}{\mu}; \tag{A.4}$$

$$U_{rc} = \omega r \tag{A.5}$$

where r is the radius of the rotating cylinder, and ω is the rotational speed of the cylinder.
Mass transfer correlation [16]:

$$Sh_{rc} = 0.079 {Re_{rc}}^{0.7} Sc^{0.356}; \qquad 1000 \leq Re_{rc} \leq 100{,}000 \tag{A.6}$$

$$Sh_{rc} = \frac{2kr}{D} \tag{A.7}$$

Gas-liquid flow model

Flow pattern determination:

The boundary for stratified/non-stratified flow (line 1 in Figure 1) can be estimated using the approach of Kelvin-Helmholtz instability of interfacial waves suggested by Taitel and Dukler [28]. The boundary slug/annular flow (line 2 in Figure 1) can be computed using the criterion suggested by Barnea [2] of liquid holdup (α_l) larger or equal to 0.24 for intermittent flow. The boundary dispersed bubble/slug flow (line 3 in Figure 1) can be calculated using the criterion $d_{max} \leq d_{crit}$ suggested by Brauner [29], where d_{max} is the maximum bubble size in the flow and d_{crit} is a critical bubble size based on the balance of turbulent and buoyant forces and excessive deformation of dispersed bubbles. Line 4 in Figure 1 is computed from the maximum gas holdup that can be entrained in the liquid phase ($\alpha_{gmax} = 0.52$) as suggested by Taitel et al. [30]. A region of "bubble" flow pattern, between dispersed bubble and intermittent flow, can also exist in inclined and vertical pipes [30, 31]. The boundary bubble/slug flow can be determined by a critical gas holdup or void fraction ($\alpha_{gcrit} = 0.25$) as suggested in [31]; thus, bubbly flow occurs if $\alpha_g < \alpha_{gcrit}$, and intermittent flow happens when $\alpha_g \geq \alpha_{gcrit}$.

Slug flow characteristics:

The gas pocket/liquid film region of the slug unit can be modeled by using the combined momentum balance at steady state for stratified liquid and gas in a pipe based on the simplified geometry shown in Figure A.1:

$$\frac{\tau_{gf} S_{gf}}{\alpha_{gf}} - \frac{\tau_{lf} S_{lf}}{\alpha_{lf}} + \tau_i S_i \left(\frac{1}{\alpha_{lf}} + \frac{1}{\alpha_{gf}}\right) - A\left(\rho_l - \rho_g\right) g \sin\beta = 0 \tag{A.8}$$

where τ_{gf} and τ_{lf} are the wall shear stresses due to the flow of the gas bubble and the liquid film, respectively; τ_i is the shear stress at the gas-liquid interface, α_{gf} (also expressed as: $1-\alpha_{lf}$) and α_{lf} are the fractions of pipe cross sectional area (A) occupied by gas and liquid, respectively; S_{gf} and S_{lf} are the pipe perimeters wetted by gas and liquid, respectively; S_i is the perimeter of the gas-liquid interface, ρ_g is the gas density; g is the gravitational acceleration, and β is the pipe inclination angle measured from the horizontal. The wall shear stresses are calculated as follows:

$$\tau_{gf} = \frac{1}{2} f_{gf} \rho_g {u_{gf}}^2 \tag{A.9}$$

$$\tau_{lf} = \frac{1}{2} f_{lf} \rho_l {u_{lf}}^2 \tag{A.10}$$

and the interfacial stress:

$$\tau_i = \frac{1}{2} f_i \rho_g \left(u_{gf} - u_{lf}\right)\left|u_{gf} - u_{lf}\right| \tag{A.11}$$

where u_{gf} and u_{lf} are the mean velocities of the gas and liquid; respectively; and f_{gf}, f_{lf} and f_i are the friction factors for the gas bubble, liquid film and gas-liquid interface, respectively. Friction factors are estimated as:

$$f = C_f Re^{-n_f} \tag{A.12}$$

where Re is the Reynolds number, and C_f and n_f are constants equal to 0.046 and 0.2, respectively; for turbulent flow Re > 2100, and 16 and 1 for laminar flow $Re \leq 2100$. In case the pipe surface is not hydraulically smooth, the explicit friction factor formulas in [32] can be used. The Reynolds numbers for the gas bubble and liquid film flows are:

$$Re_g = \frac{\rho_g u_{gf} d_{gf}}{\mu_g} \tag{A.13}$$

$$Re_{lf} = \frac{\rho_l u_{lf} d_{lf}}{\mu_l} \tag{A.14}$$

and gas-liquid interface:

$$Re_i = \frac{\rho_g \left|u_{gf} - u_{lf}\right| d_{gf}}{\mu_g} \tag{A.15}$$

where μ_g and μ_l are the viscosities of the gas and the liquid, respectively; d_{gf} is the hydraulic diameter for the gas bubble flow:

$$d_{gf} = \frac{4A\alpha_{gf}}{S_{lg} + S_i} \tag{A.16}$$

and d_{lf} is the hydraulic diameter of the liquid film flow:

$$d_{lf} = \frac{4A\alpha_{lf}}{S_{lf}} \tag{A.17}$$

The mean velocity of the liquid slug cylinder is approximated to the mixture velocity, which is calculated as the summation of superficial gas and liquid velocities:

$$u_{\mathrm{m}} = u_{\mathrm{sg}} + u_{\mathrm{sl}} \tag{A.18}$$

No slip is considered between the entrained gas bubbles and the liquid in the slug cylinder. Then, the velocities of the gas bubble and the liquid film can be related with the gas bubble and liquid film holdups (α_{gf} and α_{lf}, respectively) as suggested by Dukler and Hubbard [33]:

$$u_{\mathrm{gf}} = u_{\mathrm{t}} + (u_{\mathrm{m}} - u_{\mathrm{t}}) \left(\frac{1-\alpha_{\mathrm{ls}}}{1-\alpha_{\mathrm{lf}}}\right) \tag{A.19}$$

$$u_{\mathrm{lf}} = u_{\mathrm{t}} \left(1 - \frac{\alpha_{\mathrm{ls}}}{\alpha_{\mathrm{lf}}}\right) + u_{\mathrm{m}} \frac{\alpha_{\mathrm{ls}}}{\alpha_{\mathrm{lf}}} \tag{A.20}$$

where α_{ls} is the liquid holdup at the slug cylinder, and u_{t} is the translational velocity at which the slug propagates, and is estimated as:

$$u_{\mathrm{t}} = C_0 u_{\mathrm{m}} + u_{\mathrm{b}} \tag{A.21}$$

where u_{b} (m/s) is the Taylor bubble velocity that can be neglected in horizontal slug flow, C_0 is the distribution parameter used in the drift-flux model and can be approximated with the value 1.2 [34].
The liquid holdup at the slug cylinder is approximated using the Gregory et al. correlation [35]:

$$\alpha_{\mathrm{ls}} = \left[1 + \left(\frac{u_{\mathrm{m}}}{8.66}\right)^{1.39}\right]^{-1} \tag{A.22}$$

The constant 8.66 in equation above has SI velocity units.

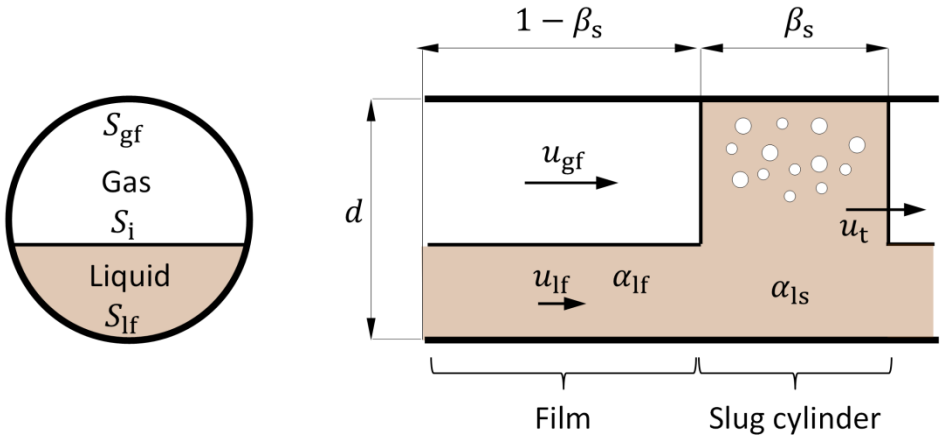

Figure A.1. Schematic representation of the slug flow unit assumed in the gas-liquid model.

The combined momentum balance in equation (A.8) can be solved iteratively to find the liquid film holdup (α_{lf}). Since equation (A.8) has multiple roots for pipe inclination angles (β) different than zero; in general, the smaller root is considered as solution of the problem.

From the conservation of the liquid mass in the slug unit (liquid film + slug cylinder), the relative length of the slug cylinder is estimated in terms of the superficial liquid velocity and the velocities and the liquid holdups of the film and the slug cylinder:

$$\beta_s = \frac{u_{sl} - u_{lf}\,\alpha_{lf}}{u_m \alpha_{ls} - u_{lf}\,\alpha_{lf}} \tag{A.23}$$

Then, the average liquid holdup in the slug unit is:

$$\alpha_l = \alpha_{ls}\,\beta_s + \alpha_{lf}\,(1 - \beta_s) \tag{A.24}$$

The shear stress at the liquid slug is estimated as:

$$\tau_{ls} = \frac{1}{2} f_{ls} \rho_{ls} {u_t}^2 \tag{A.25}$$

The friction factor f_{ls} is calculated as in (A.12) but using the Reynolds number $\rho_{ls} u_t d/\mu_{ls}$, where the density and viscosity of the liquid slug are:

$$\rho_{ls} = \rho_l \alpha_{ls} + \rho_g\,(1 - \alpha_{ls}) \tag{A.26}$$

$$\mu_{ls} = \mu_l \alpha_{ls} + \mu_g\,(1 - \alpha_{ls}) \tag{A.27}$$

Stratified and annular flow characteristics:

The combined momentum equation (A.8) is also used to calculate flow characteristics in stratified and annular flow. In the case of the latter, the liquid is assumed to occupy mostly the pipe bottom (as shown in Figure A.1) for inclination angles of absolute value smaller than 45 degrees. For relatively high gas velocities, a fraction of the liquid can be entrained by the gas flow, which can be calculated as [36]:

$$E = \left\{1 - \exp\left[-0.125\left(10^4 \frac{u_{sg}\mu_g}{\sigma}\sqrt{\frac{\rho_g}{\rho_l}} - 1.5\right)\right]\right\} \tag{A.28}$$

Then, the liquid holdup is:

$$\alpha_l = \alpha_{lf} + \frac{u_{sl} E}{(u_{sg} + u_{sl} E)} \tag{A.29}$$

Note that if E=0 then $\alpha_l = \alpha_{ls}$. If E>0, the gas holdup (α_{gf}) in equation (A.8) is now the holdup of a combined gas-liquid flow. The velocity of the liquid film is:

$$u_{lf} = \frac{u_{sl}(1-E)}{\alpha_{lf}} \tag{A.30}$$

The velocity of the gas or gas-liquid mix (E>0, no slip between the entrained liquid drops and the gas) is:

$$u_{gf} = \frac{(u_{sg} + u_{sl} E)}{\alpha_{gf}} \tag{A.31}$$

When solving equation (A.8) a different interfacial friction closure relationship is used instead of equation (A.11):

$$\tau_{\mathrm{i}} = \frac{1}{2} f_{\mathrm{i}} \rho_{\mathrm{gf}} \left(u_{\mathrm{gf}} - u_{\mathrm{i}}\right) \left|u_{\mathrm{gf}} - u_{\mathrm{i}}\right| \tag{A.32}$$

where u_{i} is the velocity of the interface between the liquid film and the gas calculated as in Oliemans et al. [37]. The interfacial friction factor (f_{i}) is calculated with the Colebrook equation using an effective roughness described in [37], the hydraulic diameter (d_{gf}) and the Reynolds number $\rho_{\mathrm{gf}} u_{\mathrm{gf}} d_{\mathrm{gf}} / \mu_{\mathrm{gf}}$, where:

$$\rho_{\mathrm{gf}} = \rho_{\mathrm{l}} \left(1 - \alpha_{\mathrm{gr}}\right) + \rho_{\mathrm{g}} \alpha_{\mathrm{gr}} \tag{A.33}$$

$$\mu_{\mathrm{gf}} = \mu_{\mathrm{l}} \left(1 - \alpha_{\mathrm{gr}}\right) + \mu_{\mathrm{g}} \alpha_{\mathrm{gr}} \tag{A.34}$$

$$\alpha_{\mathrm{gr}} = \frac{u_{\mathrm{sg}}}{\left(u_{\mathrm{sg}} + u_{\mathrm{sl}} E\right)} \tag{A.35}$$

Dispersed bubble and Bubble flow characteristics:

A homogeneous no-slip model is used to estimate flow characteristics in dispersed bubble flow. Therefore, the velocity of the liquid and the entrained gas bubbles is considered to be similar to the mixture velocity:

$$u_{\mathrm{l}} = u_{\mathrm{g}} \cong u_{\mathrm{m}} \tag{A.36}$$

The liquid holdup is:

$$\alpha_{\mathrm{l}} = \frac{u_{\mathrm{sl}}}{\left(u_{\mathrm{sg}} + u_{\mathrm{sl}}\right)} \tag{A.37}$$

The wall shear stress is:

$$\tau_{\mathrm{l}} = \frac{1}{2} f_{\mathrm{m}} \rho_{\mathrm{m}} {u_{\mathrm{l}}}^2 \tag{A.38}$$

where the friction factor f_{m} is calculates as in (A.12) using the Reynolds number $\rho_{\mathrm{m}} u_{\mathrm{l}} d / \mu_{\mathrm{m}}$, where:

$$\rho_{\mathrm{m}} = \rho_{\mathrm{l}} \alpha_{\mathrm{l}} + \rho_{\mathrm{g}} \left(1 - \alpha_{\mathrm{l}}\right) \tag{A.39}$$

$$\mu_{\mathrm{m}} = \mu_{\mathrm{l}} \alpha_{\mathrm{l}} + \mu_{\mathrm{g}} \left(1 - \alpha_{\mathrm{l}}\right) \tag{A.40}$$

Bubble flow can have significant slip between the liquid and the gas bubbles which rise quicker due to buoyancy. In this case, drift flux model can be used to properly determine the liquid and gas holdups. Equations (A.38 to A.40) can then be used to calculate flow characteristics.

References

1. R. Baldwin, Black Powder in the Gas Industry-Sources, Characteristics and Treatment Mechanical and Fluids Engineering Division, Southwest Research Institute, San Antonio TX (1997) TA 97-94.
2. D. Barnea, International Journal of Multiphase Flow, **13** (1987) 1.
3. S. Nešić, A. Kahyarian, Y.S. Choi, Corrosion, **75** (2019) 274.
4. Y. Zheng, J. Ning, B. Brown, S. Nešić, Corrosion, **72** (2016) 679.
5. M. Langsholt, M. Nordsveen, K. Lunde, S. Nesic, J. Enerhaug, Wall Shear Stress and Mass Transfer Rates – Important Parameters in CO_2 Corrosion, BHR Group Multiphase 97', Cannes, France (1997) pp. 537-552.
6. N. Pecherkin, V. Chekhovich, Mass Transfer in Two-Phase Gas-Liquid Flow in a Tube and in Channels of Complex Configuration, in: Mass Transfer in Multiphase Systems and its Applications, Ed. M. El-Amin, InTech, Croatia (2011) pp. 155-178.
7. H. Wang, H.D. Dewald, W.P. Jepson, Journal of The Electrochemical Society, **151** (2004) 114.
8. H. Wang, T. Hong, J.-Y. Cai, W.P. Jepson, Enhanced Mass Transfer and Wall Shear Stress in Multiphase Slug Flow, NACE Corrosion 2002, Houston TX (2002) Paper 2501.
9. H. Wang, D. Vedapuri, J.Y. Cai, T. Hong, W.P. Jepson, Journal of Energy Resources Technology, **123** (2000) 144.
10. K. Yan, Y. Zhang, D. Che, Heat and Mass Transfer, **48** (2012) 1193.
11. F.P. Berger, K.F.F.L. Hau, International Journal of Heat and Mass Transfer, **20** (1977) 1185.
12. S. Wang, S. Nesic, On Coupling CO_2 Corrosion and Multiphase Flow Models, NACE Corrosion 2003, Houston TX (2003) Paper 3631.
13. T.H. Chilton, A.P. Colburn, Industrial & Engineering Chemistry, **26** (1934) 1183.
14. S.W. Churchill, Industrial & Engineering Chemistry Fundamentals, **16** (1977) 109.
15. D.W. Hubbard, E.N. Lightfoot, Industrial & Engineering Chemistry Fundamentals, **5** (1966) 370.
16. M. Eisenberg, C.W. Tobias, C.R. Wilke, Journal of The Electrochemical Society, **101** (1954) 306.
17. A. Kahyarian, S. Nesic, Journal of The Electrochemical Society, **166** (2019) 3048.
18. A. Kahyarian, S. Nesic, Electrochimica Acta, **297** (2019) 676.
19. C.S. Lin, R.W. Moulton, G.L. Putnam, Industrial & Engineering Chemistry, **45** (1953) 636.
20. J.T. Davies, Eddy Transfer Near Solid Surfaces, in: Turbulence Phenomena, 1st Ed., Elsevier, Netherlands (1972) pp. 121-174.
21. S.L. Gordon, J.S. Newman, C.W. Tobias, Berichte der Bunsengesellschaft für physikalische Chemie, **70** (1966) 414.
22. C. Dong, T. Hibiki, International Journal of Multiphase Flow, **108** (2018) 124.
23. C. Dong, T. Hibiki, Applied Thermal Engineering, **141** (2018) 866.
24. R.H. Notter, C.A. Sleicher, Chemical Engineering Science, **26** (1971) 161.
25. S. Aravinth, International Journal of Heat and Mass Transfer, **43** (2000) 1399.
26. K.E. Kee, M. Babic, S. Richter, L. Paolinelli, W. Li, S. Nesic, Flow Patterns and Water Wetting in Gas-Oil-Water Three-phase Flow – A Flow Loop Study, NACE Corrosion 2015, Houston TX (2015) Paper 6113.
27. L.D. Paolinelli, Study of Phase Wetting in Three-Phase Oil-Water-Gas Horizontal Pipe Flow - Recommendations for Corrosion Risk Assessment, NACE Corrosion 2018, Houston TX (2018) Paper 11213.
28. Y. Taitel, A.E. Dukler, AIChE Journal, **22** (1976) 47.

29. N. Brauner, International Journal of Multiphase Flow, **27** (2001) 885.
30. Y. Taitel, D. Bornea, A.E. Dukler, AIChE Journal, **26** (1980) 345.
31. D. Barnea, O. Shoham, Y. Taitel, A.E. Dukler, Chemical Engineering Science, **40** (1985) 131.
32. S.E. Haaland, Journal of Fluids Engineering, **105** (1983) 89.
33. A.E. Dukler, M.G. Hubbard, Industrial & Engineering Chemistry Fundamentals, **14** (1975) 337.
34. K.H. Bendiksen, D. Maines, R. Moe, S. Nuland, SPE Production Engineering, **6** (1991) 171.
35. G.A. Gregory, M.K. Nicholson, K. Aziz, International Journal of Multiphase Flow, **4** (1978) 33.
36. G.B. Wallis, One-Dimensional Two-Phase Flow, Mc Graw-Hill, New York (1969) pp. 318-321.
37. R.V.A. Oliemans, B.F.M. Pots, N. Trompé, International Journal of Multiphase Flow, **12** (1986) 711-732.